

# X-ray and Optical Filaments in M87

William B. Sparks, Megan Donahue

*Space Telescope Science Institute, 3700 San Martin Drive, Baltimore, MD 21218*

and

Andrés Jordán,<sup>1</sup> Laura Ferrarese, Patrick Côté

*Dept. of Physics & Astronomy, Rutgers University, 136 Frelinghuysen Road, Piscataway, NJ 08854.*

## ABSTRACT

We compare a very deep X-ray image of M87, at the center of the Virgo Cluster, to high-quality optical images of the low excitation emission-line gas in the same region. There are striking coincidences of detail between the two. We explore the possibility that this represents a thermal interaction between hot gas at  $10^7$  K and warm gas at  $10^4$  K. We find two temperatures are present in the X-ray gas, with the lower more prevalent in the vicinity of the optical filaments. Electron conduction from the hot phase to the cooler one provides a quantitatively acceptable energy source for the optical filaments, and we show additionally that it can do so for the brightest X-ray cluster, Perseus. If operative, conduction in the presence of gas-rich galaxy mergers, may explain the presence of “cool cores” in clusters of galaxies.

*Subject headings:* galaxies: individual (M87), galaxies: ISM, X-rays: galaxies: clusters

## 1. Introduction

Recent observations with the new generation of X-ray satellites, XMM-Newton and Chandra, have shown that the conventional cooling-flow theory (Fabian 1994) is no longer tenable. Data from XMM-Newton has revealed that while there is relatively cool X-ray

---

<sup>1</sup>Claudio Anguita Fellow

emitting gas in the centers of galaxy clusters, there is an absence of predicted cooler gas below  $\sim 10^7$  K (Molendi & Pizzolato 2001, Böhringer et al. 2002, Matsushita et al. 2002, Molendi 2002, Donahue & Voit 2003). Two mechanisms in particular have been invoked to compensate for energy lost through X-ray radiation, namely heating by an intermittently active nucleus (e.g. Tucker & Rosner 1983, Reynolds et al. 2001, Ruszkowski & Begelman 2002, Kaiser & Binney 2003) and thermal electron conduction of heat into the inner regions from the vast reservoir of thermal energy in the cluster e.g. Tucker & Rosner 1983, Rosner & Tucker 1989, Sparks, Macchetto, & Golombek 1989, Sparks 1992, Voigt et al. 2002, Fabian, Voigt, & Morris 2002, Zakamska & Narayan 2003).

The Virgo cluster of galaxies is the nearest cluster with substantial X-ray emission, hosting a small but typical cool core and the well-studied active radio galaxy M87. XMM-Newton spectroscopy of the core of the Virgo cluster was amongst the pivotal work that showed large amounts of cooling gas are not present. The lower limit to the temperature found by XMM-Newton was 0.8 keV, or  $0.9 \times 10^7$  K (Molendi 2002). The proximity of M87, 16.1 Mpc (Tonry 2001), makes it an attractive target for detailed physical studies, with spatial resolution of 1 arcsec corresponding to 77 pc. Here, we describe a very deep Chandra X-ray image and show that it displays a wealth of fine structure on the arcsec scale. Comparison with optical images reveals that these filaments are closely related to the  $H\alpha + [NII]$  emitting warm gas at  $T \sim 10^4$  K. This in turn suggests interaction between two very different gas phases, and hence provides clues to the physical transport processes operating in the cluster center.

From an optical perspective, the emission filament system was studied by Sparks, Ford, & Kinney (1993), and earlier, by Ford & Butcher (1979). Sparks et al. (1993) found that the emission filaments are dusty, that the innermost ones are likely to be outflowing due to interaction with the jet, but that the outer filaments are infalling. The overall excitation state is low, typical of filament systems in elliptical galaxies and galaxy clusters. The kinematics and geometry inferred from the dustiness and correlation with radio source structures led Sparks et al. (1993) to propose that the filaments have their origin in a small merger event. Weil, Bland-Hawthorn & Malin (1997) found evidence of diffuse low surface brightness light in M87 at large radii to the Southeast, which they interpreted as tidal debris of a recent encounter.

Young, Wilson, & Mundell (2002) presented an analysis of a 40 ks Chandra X-ray image of the Virgo cluster. They showed that the central regions are cooler than the outer parts of the cluster, and that there are localized cool regions associated with the complex radio source of M87, with its jet, inner lobes, intermediate lobes, and outer, apparently buoyant, relic radio structure. Young et al. (2002) further showed that the X-ray structures to the

North and East of the nucleus correlate with optical  $H\alpha + [NII]$  filaments, and that the X-ray gas was coolest in the vicinity of the optical filaments.

Here we present a  $\sim 150$  ks Chandra X-ray image,  $\sim 4\times$  longer integration than the Young et al. (2002) data. With this improved  $S/N$ , we show a much clearer view of the X-ray filaments and the detail within them, and hence reveal with greater clarity the nature of the correlation between the optical and X-ray emission. We also utilize the spectral information of the new data to probe the physical conditions within the filaments compared to their surroundings. Motivated by an earlier suggestion that electron conduction from the hot gas into the cold gas of an accretion or merger event can explain the peculiar symptoms of a “cooling flow” (Sparks et al. 1989), we assess whether this mechanism could provide the energy to ionize the filament system.

## 2. Observations

### 2.1. Chandra X-ray observations

To create an X-ray image with high signal-to-noise we merged the three longest Chandra ACIS-S observations of the Virgo cluster. The relative astrometry of the observations, based on inspection of point sources detected in all three observations, showed that no shifts or rotations were required to stack the data. Level-1 CTI-corrected event files were generated by running *acis\_process\_events* (CIAO 2.3). Level-2 event files were created by selecting events with grades 0 2 3 4 6, and status of 0. The “good time intervals” supplied by the original pipeline were used. We then examined a light curve from the S3 chip and omitted data obtained during observation periods affected by major flares. We then merged all three independent observations, and a final event file was created from a subset of the merged file by retaining only the 0.3–3.0 keV events from the S3 back-illuminated CCD. An exposure map for the merged observation was created assuming a monochromatic incident spectrum of 1.5 keV. The resulting map has units  $\text{photons s}^{-1} \text{ cm}^{-2} \text{ pixel}^{-1}$  and pixel size  $0.492'' \times 0.492''$ . A summary of the observations is reported in Table 1. The total useful exposure time of the final image is  $\approx 154$  ks.

### 2.2. Narrow-band Optical Imaging

For morphological comparison, we use the ESO/NTT 3000 sec  $H\alpha + [NII]$  image of Macchetto et al. (1996). The image was constructed from two separate exposures of 1500 sec each obtained on the ESO 3.4-m NTT, and processed in the conventional fashion as described

in Macchetto et al. (1996). Continuum subtraction was performed using a long  $R$ -band exposure. This long exposure was saturated in the central regions, and displayed a low-level ghost weakly visible in Fig. 1. These qualities do not affect a morphological comparison. To carry out a quantitative flux calibration, we used the lower signal-to-noise, but well-calibrated image from KPNO presented in Sparks et al. (1993). That image was constructed from  $5 \times 120$  sec exposures and the reduction procedures and flux calibration are documented in Sparks et al. (1993).

### 3. Morphology and Morphological Comparisons

Fig. 1 shows the new, high  $S/N$  X-ray image. The image has been adaptively smoothed to retain a  $S/N = 10$  per pixel, and is displayed on a logarithmic scale. There is a wealth of detail and filamentary structure as well as arcs, edges and voids within the hot gas.

For comparison to the optical line-emitting gas, we resampled the optical and X-ray images to be spatially registered and blinked between them. Fig. 2 shows the X-ray image next to the  $H\alpha + [NII]$  image, and labels some of the features common to both (given in boldface in the text). Beginning in the Southeast corner, the knotty complex of  $H\alpha + [NII]$  emission coincides with the outer edge of the Southeast inner radio lobe (Sparks et al. 1993). The X-ray emission shows a similar complex, also brightest on the edge closest to the nucleus. Just North of this complex, where optical filaments appear to cross, we see both brighter optical emission and a knot in the X-ray emission. To the East of the knot the optical emission diverges from this point in a double strand, and fades, as also does the X-ray emission. From the knot, the  $H\alpha + [NII]$  filament runs almost straight North-West and then kinks to run East-West. The same behavior is present in the X-ray image. Moving to the East, the filaments brighten in a bar as they converge with an arc located to the East of the nucleus. This arc of emission ends at a bright knot South of the nucleus. North of the nucleus and emerging from it, there is a very bright loop of emission, also in both images, reminiscent of a Solar coronal loop.

There are a few places where the maps differ: to the Southwest of the nucleus, there are X-ray knots without optical counterparts, while the  $H\alpha + [NII]$  filaments due West of the tip of the jet have little or no X-ray counterpart. The bright optical filament near the jet running Northwest does not have a strong X-ray counterpart. Also, the flux ratios are not identical even where the morphology is similar. Overall, however, there are clear coincidences in shape and distribution between the two datasets.

This is a similar situation to that found in the Perseus Cluster by Fabian et al. (2003)

where optical filaments also have unambiguous counterparts in a very deep X-ray image.

## 4. Discussion

### 4.1. Physical properties inferred from X-ray data

In order to compare physical conditions in the filaments and inter-filament regions, we extracted X-ray events from 6 apertures from the longest single observation of 98,664 seconds (OBSID 2707). Fig. 4 shows the apertures used, each having between 2,000 and 10,000 X-ray counts total, and  $> 25$  counts per spectral element. B1 and B2 are box shaped and lie on bright X-ray features with counterparts in the  $H\alpha$  image. C1–4 are circular and lie at nearly the same distance from the nucleus, but are not on bright filamentary features. A small correction was made for background contamination and weighted RMF and ARF files were created for each aperture. XSPEC 11.2.0 was used to analyze the resulting spectra. The HI column was kept fixed at  $1.8 \times 10^{20} \text{ cm}^{-2}$  (Lieu et al. 1996). The spectral fits are summarized in Table 2. All required two temperature components, and we fitted a two-temperature MEKAL model with a single metallicity for both components. Densities were computed assuming pressure equilibrium. Quoted uncertainties are 90% confidence intervals based on propagated statistical errors only. The emission was assumed to arise from a spherical volume defined by the circular apertures and from a cylindrical volume defined by the elongated box apertures, and we neglected projection through the cluster (Molendi 2002). To provide a visual sense of the X-ray spectral data, we also constructed a red/green/blue image using X-ray passbands from 0.5 to 1 keV (red), 1 to 2 keV (green) and above 3 keV (blue), shown in Fig. 5. The filaments are more pronounced in the lower energy bands, revealing this with their redder color in Fig. 5 and indicative of a lower mean temperature within the filaments.

The detailed spectral fits find two temperature components within the X-ray plasma, 0.8 and 1.6 keV, consistent with earlier findings of Young et al. (2002), Molendi (2002), for *both* the filament and inter-filament regions. Interestingly, the temperature values for the two regions are the same within the uncertainties. What differs, though, is the relative proportion of cool and hot gas. In the  $H\alpha$  filaments, the cool-gas filling factor is of order twice that of the inter-filament region. The pressures derived from the X-ray fitting,  $0.6\text{--}2.5 \times 10^{-9} \text{ dynes cm}^{-2}$ , are very comparable to those derived from optical observations (Heckman et al. 1989),  $0.6\text{--}2.4 \times 10^{-9} \text{ dynes cm}^{-2}$ .

#### 4.2. Conduction as an energy source for the optical filaments

Sparks et al. (1989), primarily based on optical observations of the dusty emission filaments in the Centaurus Cluster of galaxies (NGC 4696), proposed that cool, merging gas falling into a hot X-ray corona could be energized by thermal conduction from the hot phase. This would cause optical line emission from the cooler gas and locally enhance the X-ray emission. The two phases should consequently display spatial similarities. Cowie & McKee (1977) pointed out that if temperature gradients are sufficiently high, classical electron conduction (Spitzer 1962) overestimates the actual energy flux. The heat conductivity “saturates” and is limited by the electrons available to cross a surface. This could arise for example if the system is in an unrelaxed dynamic, transient state, or if length scales are smaller than a critical value, related to the electron mean free path.

To see if conduction can provide a plausible energy source for the optical line emission, we note that the fraction of energy emitted as  $H\alpha + [NII]$  line radiation is expected to be of order 2–6% of the total optical line cooling (Voit et al. 1994). Allowing for energy losses from the interface radiation and to infrared emission of heated dust, we assume  $\sim 1\%$  of the available heat energy re-emerges as  $H\alpha + [NII]$ . The topology of the filament system is unknown, however the surface area is at least twice the projected surface area (front and back) and is potentially much higher, e.g. if the filaments are “clouds” of small blobs, so conservatively we assume the actual area is  $3\times$  the apparent. The saturated heat conductive flux per unit area is

$$q_{sat} = 0.4 \left( \frac{2kT_e}{\pi m_e} \right)^{1/2} n_e kT_e \approx 0.0542 T_7^{3/2} n_{0.1} \text{ erg s}^{-1} \text{ cm}^{-2} \quad (1)$$

where  $T_7 = T_e/10^7\text{K}$  and  $n_e$  is the electron density, with  $n_{0.1} = n_e/0.1 \text{ cm}^{-3}$ . The classical Spitzer heat flux per unit area is

$$q = \kappa \nabla T \approx 0.55 T_7^{7/2} / L_{pc} \text{ erg s}^{-1} \text{ cm}^{-2} \quad (2)$$

For a temperature  $T \approx 10^7 \text{ K}$  and an electron density  $\approx 0.1 \text{ cm}^{-3}$ , the conductivity saturates if the length scale is  $\sim 10 \text{ pc}$ . In M87, the X-ray filaments and optical filaments appear marginally resolved, although since we may be viewing sheets or ribbons, the interface length scale could be smaller. For reference, we adopt a length scale of  $L \sim 100 \text{ pc}$  at 20 arcsec radius, and assume it is inversely proportional to radius. Two temperatures are needed to describe the X-ray gas in M87, see above and Molendi (2002). The lower has  $T \approx 0.7$ – $0.9 \text{ keV}$  and the higher  $\approx 1.4$ – $1.6 \text{ keV}$ , and since the  $H\alpha + [NII]$  filaments are associated with a higher proportion of cooler gas (§ 4.1, and Young et al. 2002), we adopt a temperature of  $0.9 \text{ keV}$ , and extrapolate the Northeast density profile of Young et al. (2002) inwards

for the simplest model temperature/density profile “YWM.” Kaiser (2003) develops a self-consistent entropy-based model of the hot gas in M87, which may also be transformed to a temperature/density profile. Fig. 2(a) plots the observed  $H\alpha + [NII]$  flux versus radius, with the YWM and Kaiser models in the saturated regime, and in the classical regime with the same reference length scale as above. The figure shows that saturated electron conduction can easily provide enough energy to supply the optical filaments, and that classical unsaturated conduction can too, if it is able to operate at essentially the Spitzer level for our assumed length scale. The saturated regime would be entered if the actual length scales are small ( $\sim 10$  pc). The classical domain would be valid for larger length scales, and the effectiveness of both will depend on the topology of the magnetic fields threading the system.

Fabian et al. (2003) showed that similar optical/X-ray coincidences occur in the filaments of the Perseus Cluster (NGC1275). The X-ray filaments are  $< \sim 500$  pc in width, the inner temperature is  $\approx 3\text{--}4 \times 10^7$  K, and the density in the central region is  $\sim 0.05 \text{ cm}^{-3}$ . For these values, the electron conductivity is entering the saturated regime. In the absence of a definitive temperature/density profile for Perseus, we adopt two representative models, one optical and one X-ray based. Heckman et al. (1989) present a pressure profile for the center of the Perseus cluster derived from optical emission line ratios. Assuming the optical gas is in pressure equilibrium with the X-ray gas, and that the X-ray gas temperature is constant at  $T \approx 4 \times 10^7$  K, a reasonable description of their pressure profile is

$$P \approx 10^{-9} (1.36 \text{ kpc} / R)^{0.6} \text{ dyne.cm}^{-2}$$

Fabian et al. (2000, 2003) quote a steeper density dependence, based on X-ray data,  $n_e \propto 1/R$ . Hence we also include a fiducial model with that behavior, normalized to have density  $0.04 \text{ cm}^{-3}$  at a radius 1 arcmin and  $T = 3 \times 10^7$  K. Fig. 2(b) overlays saturated conductive models based on these temperature/density profiles on the optical emission filament surface brightness (Fig. 7 of Conselice et al. 2001) for Perseus. Here, we see that the saturated electron conduction predictions of these representative models, *derived from the properties of the coronal plasma only*, are remarkably close to the actual *optical data*. We conclude that, given the uncertainties, saturated electron conduction could be providing the power to the optical filament systems.

If the energy loss from the (optical/UV/IR) filament system does represent the heat being drained from the coronal phase, then it is energetically significant, overwhelming the losses due to X-rays at least locally. The energy flow rather than the total energy content dominates in this scenario, and radiation governs the ultimate loss of energy, primarily in the optical and infrared regions. The consequent cooling of the cluster core will enhance its X-ray emissivity as the density increases to maintain pressure equilibrium. The essential features of a “cool core cluster” (or cooling-flow cluster) are hence induced.

There are of course caveats to this interpretation. Topology, projection effects, magnetic fields and details of the interface impose large uncertainties on the available energy. If the cool gas is significantly in the foreground or background, then the available energy can be much less. If magnetic fields shield the filaments, the heat may not be able to flow into the filaments. Evaporating and condensing clouds in the presence of radiation and conduction have been studied by McKee & Cowie (1977) and Begelman & McKee (1990), (though we note that McKee & Cowie 1977 eliminate the important thermally stable  $10^4$  K phase from their analysis). In reality, the details of timescales, dynamical motions and inner and outer boundary conditions will all enter into a correct description of the physics of these complex regions, and it may well be that other transport processes are equally, or more, effective than electron conduction. We accept that there may indeed be other viable interpretations of the data. If indeed, it can be shown that the optical filaments are powered by a mechanism other than energy flow from the hot plasma, then we may infer that conduction would have to be suppressed since it represents a significant energy source. However, to counterbalance this, we note that the models presented above, derived from properties of the *coronal X-ray gas*, give acceptable agreement to the *optical H $\alpha$*  data, without adjustment of free parameters.

Fabian et al. (2003) draw attention to the similarity of the Perseus filaments to a rising spherical cap bubble, which has an analogue in M87: the Eastern low-frequency (intermediate) radio lobe is interacting with the halo X-ray emitting gas, and drawing it out from the center (Churazov et al. 2001). Sparks et al. (1993) showed evidence (from the velocity field plus absorption due to dust) that the innermost optical filaments of M87 are flowing out in the vicinity of the jet. Hence it may be that in such systems, the large and rapid energy release associated with the triggering of an AGN is providing, in a general sense, heating and an outflow in the central regions of the clusters, and that in both Virgo and Perseus the optical and X-ray filaments towards the center are expanding away from the nucleus, and not infalling. The outer filaments, by contrast, do appear to be infalling, and it is reasonable to speculate that the AGN activity was triggered by the same infall or merger event that is interacting with the X-ray halo. Since we are dealing in concept with fundamental physical and transport processes, if valid here, then this conclusion must have wide validity.

Given the dynamic and violent nature of cluster centers—regions that are influenced by mergers, active nuclei and energy transport processes—we suggest that the cool-core phenomenon is transient and merger induced. It is unlikely we are witnessing a steady-state even in the X-rays. If merger events have triggered nuclear activity, and if strong thermal interactions arise between hot and cold gas, then a logical consequence is that prominent X-ray peaks of cool-core galaxy clusters are themselves transient and only intermittently present as the stochastic evolution and assembly of galaxy clusters proceeds.



## 5. Conclusions

Our primary goal has been to present a very deep X-ray image of the center of the Virgo cluster, and to stress an important empirical observation, namely that warm gas with  $T \sim 10^4$  K emitting strong optical line emission is strikingly similar to a phase which is a thousand times hotter and radiates at X-ray wavelengths. This correlation may be offering important clues to the nature of transport processes in the cluster interstellar medium, since it implies that two dramatically distinct phases, close in space, “know about one another” and are in some form of thermal communication. X-ray spectral analysis shows that the hot phase itself has two temperature components, and that the lower of these is more prevalent in the vicinity of the optical filaments.

We build on these observations to show, quantitatively, that electron conduction (possibly saturated) can provide the energy seen in the form of emission line radiation in these and other optical filaments. We do not claim that this is the *only* viable model. There are important uncertainties particularly with regard to magnetic field structures and strengths, and conduction would have to proceed at or close to Spitzer or saturated levels at least in one direction. Nevertheless, the model appears promising and offers an acceptable *quantitative* relationship between  $10^7$  K coronal and  $10^4$  K plasma properties. If the material of the filaments has an external merger origin, then other ancillary properties such as their dustiness have a natural explanation.

Given the dynamic and violent nature of galaxy cluster centers, influenced by mergers, active nuclei and energy transport processes, we suggest that the cool-core phenomenon is transient and merger induced.

The Space Telescope Science Institute is operated by the Association of Universities for Research in Astronomy, Inc., under NASA contract NAS5-26555. Support for A. Jordán was provided by the National Science Foundation through a grant from the Association of Universities for Research in Astronomy, Inc., under NSF cooperative agreement AST-9613615, and by Fundación Andes under project No.C-13442. P. Coté gratefully acknowledges support for this research provided by NASA LTSA grant NAG5-11714 and funding for Chandra program CXC03400562.

## REFERENCES

- Böhringer, H., Matsushita, K., Churazov, E., Ikebe, Y., Chen, Y. 2002, A& A, 382, 804  
 Churazov, E., Brüggen, M., Kaiser, C.R., Böhringer, H., Forman, W. 2001, ApJ, 554, 261

- Conselice, C. J., Gallagher, J. S., Wyse, R. F. G. 2001, *AJ*, 122, 2281
- Cowie, L. L., McKee, C. F. 1977, *ApJ*, 211, 135
- Donahue, M., Voit, G. M., 2003, in *Clusters of Galaxies: Probes of Cosmological Structure and Galaxy Evolution*, eds. J. S. Mulchaey, A. Dressler, A. Oemler (Cambridge: CUP)
- Fabian, A. C. 1994, *ARA& A*, 32, 277
- Fabian, A. C., Sanders, J. S., Ettori, S., Taylor, G. B., Allen, S. W., Crawford, C. S., Iwasawa, K., Johnstone, R. M., Ogle, P. M. 2000, *MNRAS*, 318, 65
- Fabian, A. C., Voigt, L. M., Morris, R. G., 2002, *MNRAS*, 335, L71
- Fabian, A. C., Sanders, J. S., Crawford, C. S., Conselice, C. J., Gallagher, J. S., Wyse, R. F. G. 2003, *MNRAS* in press, astro-ph/0306039
- Ford, H. C., Butcher, H., 1979, *ApJS*, 41, 147
- Heckman, T. M., Baum, S. A., van Breugel, W. J. M., McCarthy, P. 1989, *ApJ*, 338, 48
- Kaiser, C. R., Binney, J. 2003, *MNRAS*, 338, 837
- Kaiser, C. R. 2003, *MNRAS* in press, astro-ph/0305104
- Lieu, R., Mittaz, J. P. D., Bowyer, S., Lockman, F., Hwang, C.-Y., Schmitt, J. H. M. M. 1996, *ApJ*, 458, L5
- Macchetto, F., Pastoriza, M., Caon, N., Sparks, W. B., Giavalisco, M., Bender, R., Capaccioli, M. 1996, *A& AS*, 120, 463
- Mal'ushkin, L. 2001, *ApJ*, 554, 561
- Matsushita, K., Belsole, E., Finoguenov, A. Böhringer, H. 2002, *A& A*, 386, 77
- McKee, C. F., Begelman, M. C., 1990, *ApJ*, 358, 392
- McKee, C. F., Cowie, L. L., 1977, *ApJ*, 215, 213
- Molendi, S., Pizzolato, F. 2001, 560, 194
- Molendi, S. 2002, *ApJ*, 580, 815
- Rosner, R., Tucker, W. H. 1989, *ApJ*, 338, 761
- Ruszkowski, M., Begelman, M. 2002, *ApJ*, 581, 223

- Schmidt, R. W., Fabian, A. C., Sanders, J. S. 2002, MNRAS, 337, 71
- Sparks, W. B. 1992, ApJ, 399, 66
- Sparks, W. B., Ford, H. C, Kinney, A. L, 1993, ApJ, 413, 531
- Sparks, W. B., Macchetto, F., Golombek, D., 1989, ApJ, 345, 153
- Spitzer, L. 1962, *Physics of Fully Ionized Gases* (New York: Interscience)
- Tonry, J. L., Dressler, A., Blakeslee, J. P., Ajhar, E. A., Fletcher, A. B., Luppino, G. A., Metzger, M. R., Moore, C. B., 2001, ApJ, 546, 681
- Tucker, W. H., Rosner, R. 1983, ApJ, 267, 547
- Voit, G. M., Donahue, M., & Slavin, J. D. 1994, ApJS, 95, 87
- Voigt, L. M., Schmidt, R. W., Fabian, A. C., Allen, S. W., Johnstone, R. M., 2002, MNRAS, 335, L7
- Young, A. J., Wilson, A. S., Mundell, C. G. 2002, ApJ, 579, 560
- Weil, M. L., Bland-Hawthorn, J., Malin, D. F. 1997, ApJ, 490, 664
- Zakamska, N. L., Narayan, R. 2003, ApJ, 582, 162

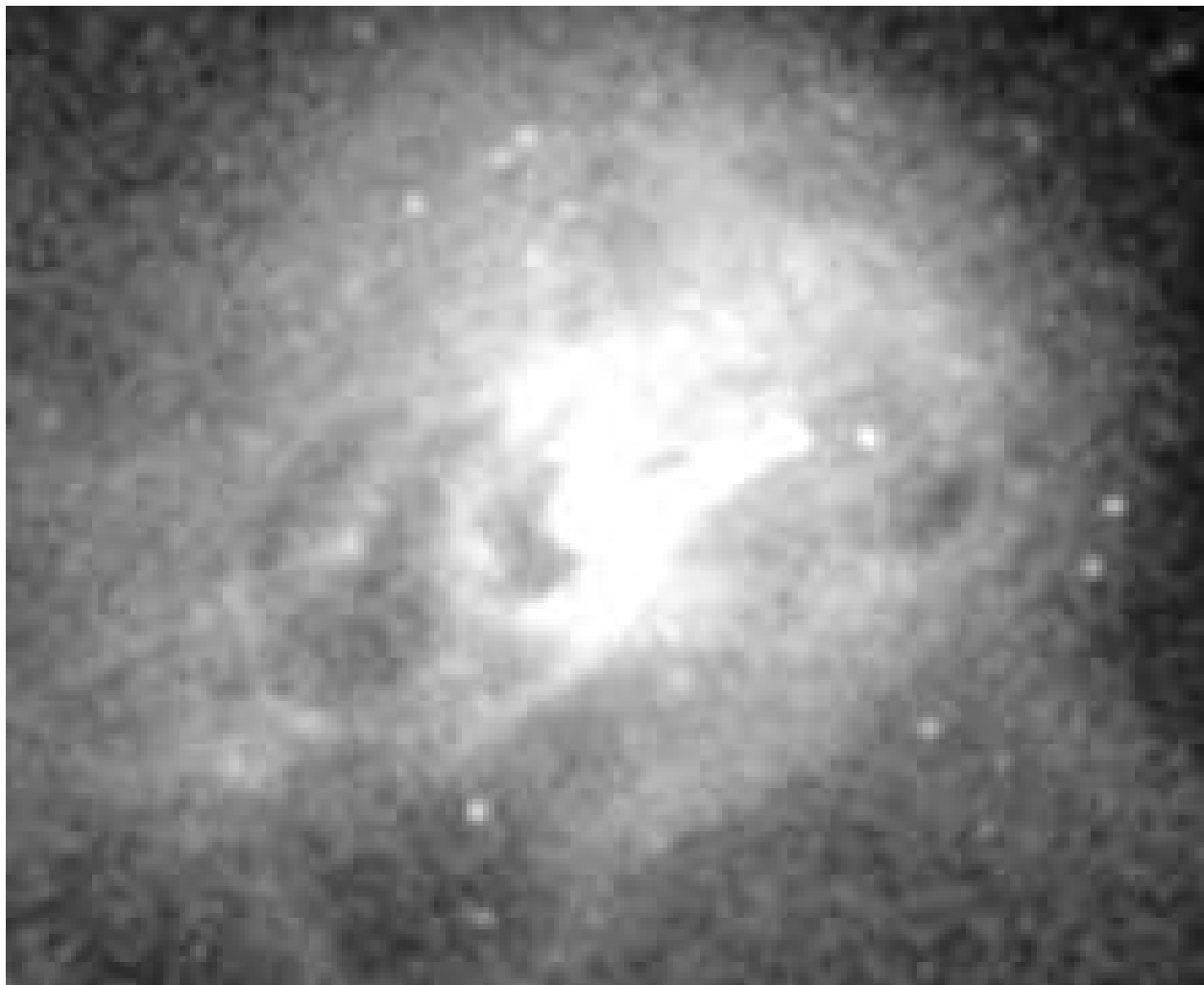


Fig. 1.— Adaptively filtered soft X-ray emission, the image is  $1.8 \times 1.5$  arcmin, North up and East to the left.

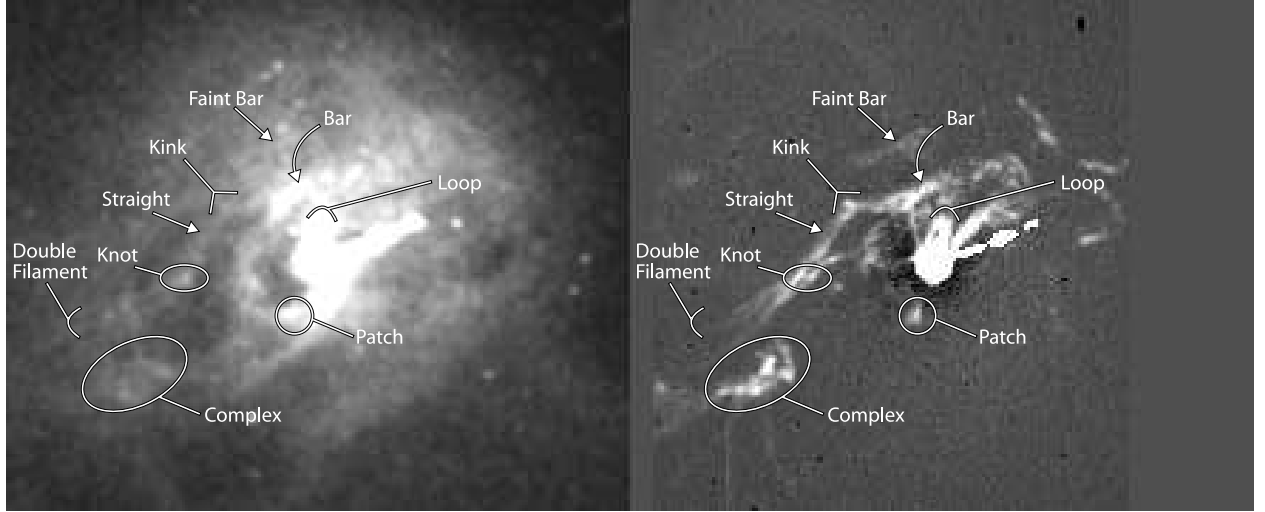


Fig. 2.— Adaptively smoothed soft X-ray emission, 154 ksec of Chandra ACIS-S observations (left), compared to the optical  $H\alpha$  +  $[NII]$  filaments system (right). The images are both  $1.8 \times 1.5$  arcmin.

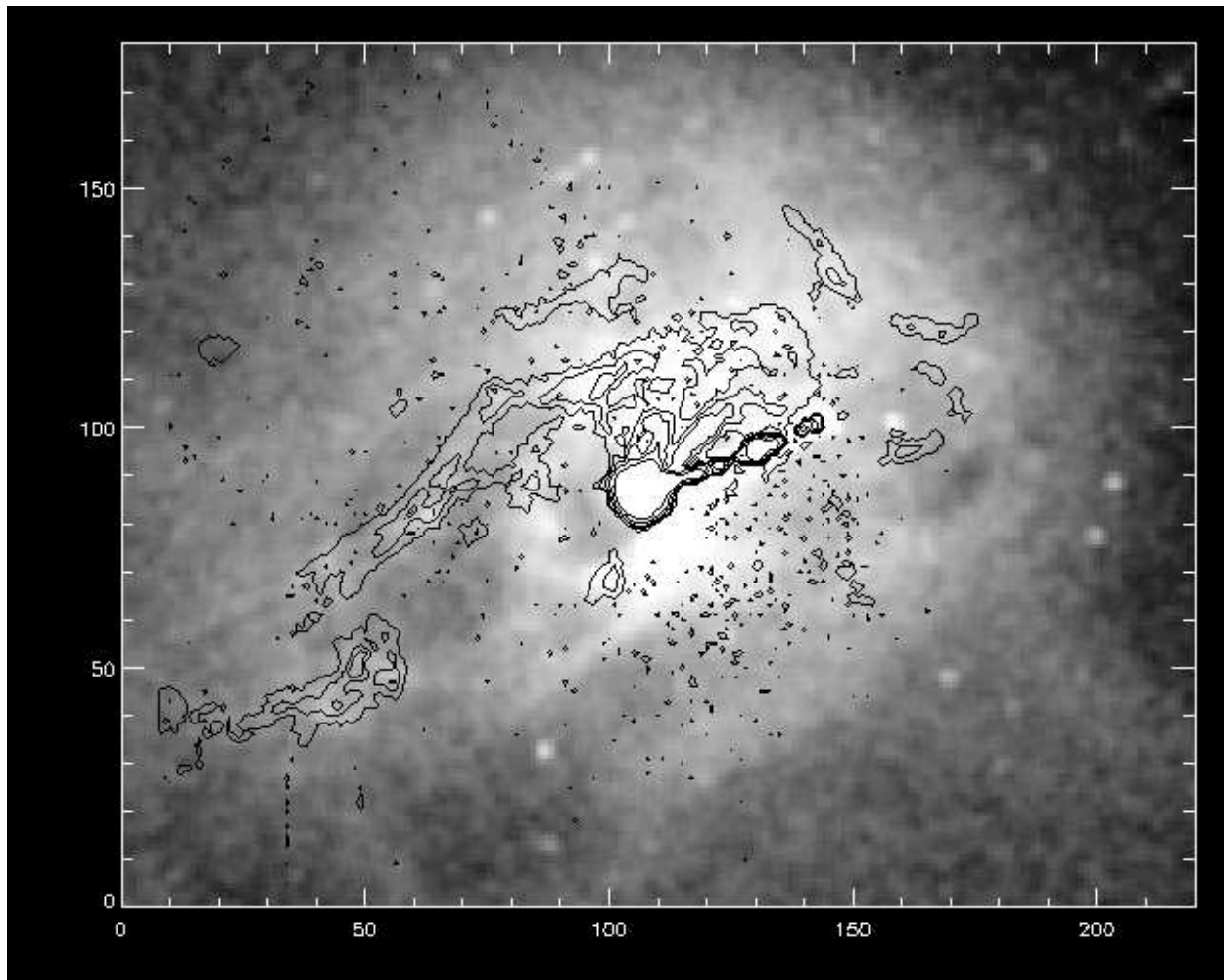


Fig. 3.— Overlay of  $H\alpha$  contours on Chandra X-ray image using the images of Figs. 1 and 2.

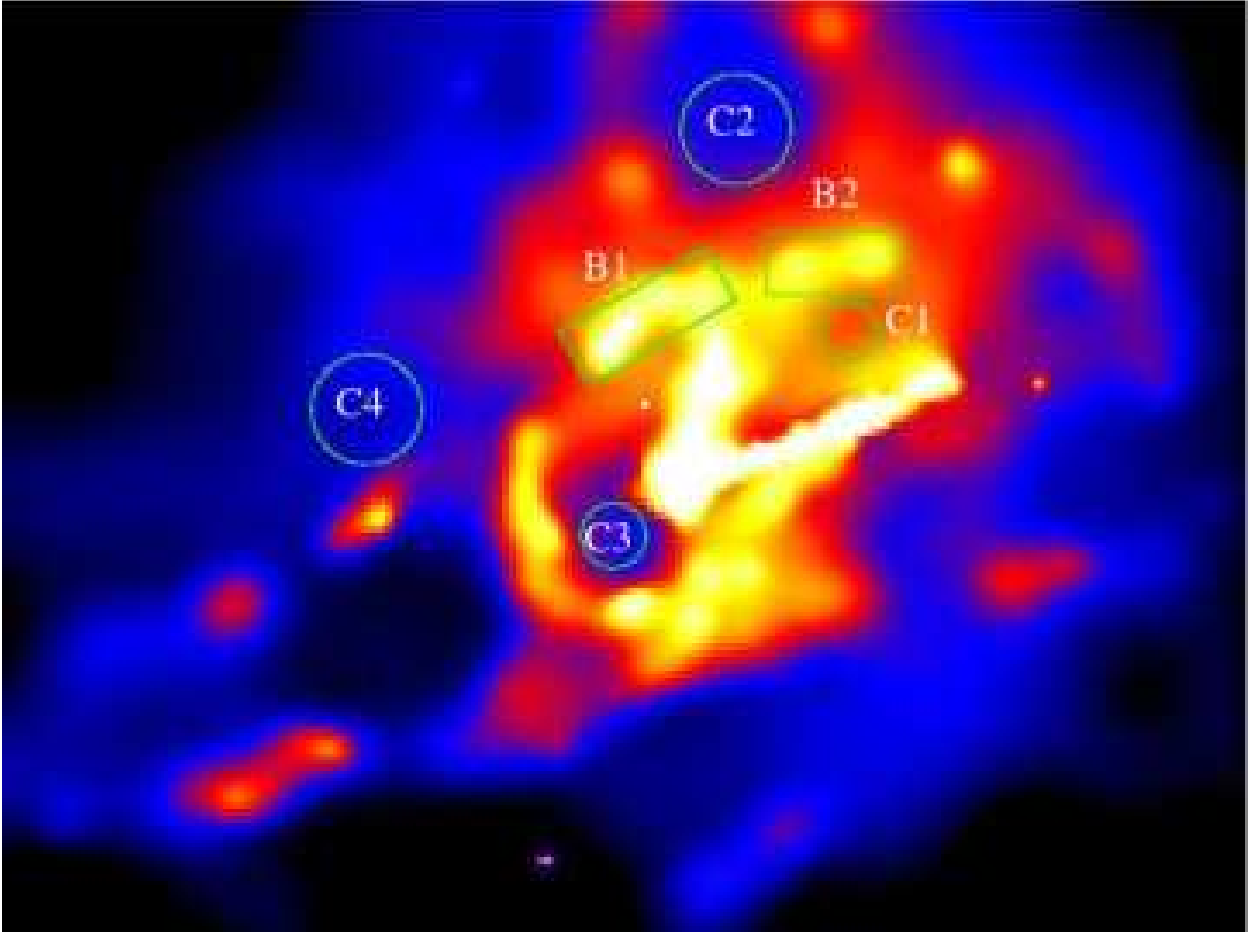


Fig. 4.— False color image of the X-ray emission of M87 showing apertures used in X-ray spectral analysis, as described in the text.



Fig. 5.— X-ray color image derived using the spectral information of the Chandra data. Redder regions, typically the regions where the filaments lie, have a more dominant cool component in the two-temperature hot gas.



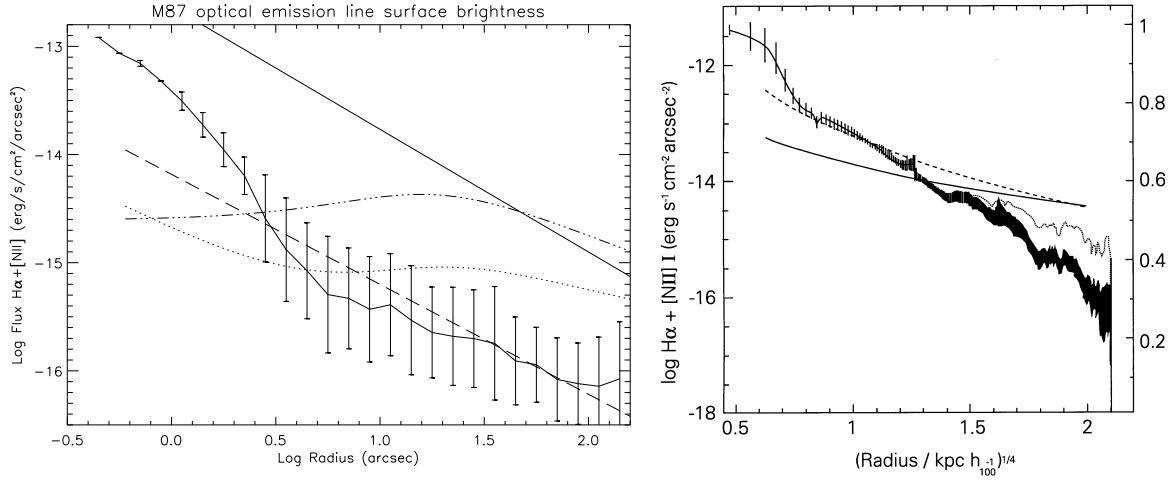


Fig. 6.— (Left) The optical  $H\alpha+[NII]$  surface brightness profile of M87 derived from Sparks, Ford & Kinney (1993). For comparison, the energy from electron conduction assuming 1% is re-radiated in these lines. Solid is YWM saturated; long dashes YWM classical for a length scale  $100(20/r \text{ arcsec}) \text{ pc}$ ; dot-dash is Kaiser saturated, dotted is Kaiser classical. (right) Two saturated conduction models for Perseus, overlaid on the  $H\alpha$  surface brightness from Fig. 7 of Conselice et al. 2002. The conduction models (running in shallow curves across the center of the diagram) are derived from inferred properties of the coronal gas and are compared to the optical observations of  $10^4 \text{ K}$  gas. The models have density  $\propto R^{-0.6}$  (solid, lower) and  $\propto R^{-1}$  (dashed, upper) curves.

Table 1. Chandra Observations of M87

Seq Num	Obs ID	Date	Original Exposure (seconds)	Useful Exposure (seconds)
700024	0352	July 29, 2000	40,000	37,112
400187	2707	July 5, 2002	23,000	18,072
400187	3717	July 6, 2002	105,000	98,664

Table 2. X-ray spectra of selected regions

Aperture name	$n_e(\text{cool})$ $\text{cm}^{-3}$	$kT_c$ keV	$n_e(\text{hot})$ $\text{cm}^{-3}$	$kT_h$ keV	$P$ $10^{-9} \text{ dynes cm}^{-2}$	$f_c$
B1	$1.18 \pm 0.08$	0.69 (0.65–0.74)	$0.56 \pm 0.06$	1.45 (1.22–1.50)	$2.5 \pm 0.3$	$0.07 \pm 0.03$
B2	$0.92 \pm 0.05$	0.82 (0.78–0.87)	$0.49 \pm 0.04$	1.54 (1.42–1.72)	$2.3 \pm 0.2$	$0.11 \pm 0.04$
C1	$0.51 \pm 0.05$	0.77 (0.71–0.83)	$0.28 \pm 0.05$	1.4 (1.26–1.56)	$1.2 \pm 0.2$	$0.11 \pm 0.05$
C2	$0.25 \pm 0.06$	0.78 (0.63–1.22)	$0.13 \pm 0.03$	1.5 (1.4–1.7)	$0.6 \pm 0.4$	$0.05 \pm 0.04$
C3	$0.64 \pm 0.10$	0.80 (0.74–0.94)	$0.32 \pm 0.06$	1.6 (1.4–2.0)	$1.6 \pm 0.3$	$0.04 \pm 0.02$
C4	$0.35 \pm 0.05$	0.87 (0.74–1.02)	$0.17 \pm 0.03$	1.8 (1.6–2.2)	$0.9 \pm 0.3$	$0.03 \pm 0.01$